CANCER

Phosphorylation of human TRM9L integrates multiple stress-signaling pathways for tumor growth suppression

Chen Gu[1], Jillian Ramos[2], Ulrike Begley[3], Peter C. Dedon[1,4]*, Dragony Fu[2]*, Thomas J. Begley[3]*

The human transfer RNA methyltransferase 9–like gene (*TRM9L*, also known as *KIAA1456*) encodes a negative regulator of tumor growth that is frequently silenced in many forms of cancer. While TRM9L can inhibit tumor cell growth in vivo, the molecular mechanisms underlying the tumor inhibition activity of TRM9L are unknown. We show that oxidative stress induces the rapid and dose-dependent phosphorylation of TRM9L within an intrinsically disordered domain that is necessary for tumor growth suppression. Multiple serine residues are hyperphosphorylated in response to oxidative stress. Using a chemical genetic approach, we identified a key serine residue in TRM9L that undergoes hyperphosphorylation downstream of the oxidative stress–activated MEK (mitogen-activated protein kinase kinase)–ERK (extracellular signal–regulated kinase)–RSK (ribosomal protein S6 kinase) signaling cascade. Moreover, we found that phosphorylated TRM9L interacts with the 14-3-3 family of proteins, providing a link between oxidative stress and downstream cellular events involved in cell cycle control and proliferation. Mutation of the serine residues required for TRM9L hyperphosphorylation and 14-3-3 binding abolished the tumor inhibition activity of TRM9L. Our results uncover TRM9L as a key downstream effector of the ERK signaling pathway and elucidate a phospho-signaling regulatory mechanism underlying the tumor inhibition activity of TRM9L.

INTRODUCTION

A tumor suppressor gene has long been suspected on the short arm of chromosome 8, given the high frequency for loss of heterozygosity within that region of many cancer genomes (*1*–*4*). One candidate for this tumor suppressor is the transfer RNA (tRNA) methyltransferase 9–like gene (*TRM9L*, also known as *KIAA1456*) located at chromosome position 8p22 (*5*). The *TRM9L* gene locus is prone to rearrangement or deletion in many types of cancer, with TRM9L expression being greatly reduced or silenced by epigenetic mechanisms in breast, bladder, colorectal, cervical, and testicular carcinomas (*5*–*8*). In further support of a tumor suppressor role for TRM9L, clinical data indicate that TRM9L expression strongly predicts prognosis, with low expression significantly correlated with early relapse or progression in breast and ovarian cancers (fig. S1) (*6*, *9*, *10*).

We have previously shown that re-expression of TRM9L in colon cancer cells reduces their proliferative capacity and confers sensitivity to the tumor environment of hypoxia (*8*). In addition to colon cancer cells, expression of TRM9L can also inhibit the proliferation, invasion, and metastasis of lung and ovarian cancer cells (*11*, *12*). In the case of colon and ovarian cancer cells, the decrease in cellular proliferation caused by TRM9L expression has been linked to increased activity of the LIN-9 tumor suppressor pathway, along with decreased hypoxia-inducible factor 1-α response to hypoxic stress (*8*, *12*). Moreover, re-expression of TRM9L can substantially reduce tumor formation in vivo, consistent with a tumor suppressor function for TRM9L (*8*). However, the specific molecular mechanisms underlying the tumor inhibition activity of TRM9L are unclear.

Mammalian TRM9L, along with its paralog, AlkB homolog 8 (ALKBH8), are predicted homologs of the *Saccharomyces cerevisiae* tRNA methyltransferase 9 (Trm9) enzyme (fig. S2A). In *S. cerevisiae*, Trm9 converts the modified wobble uridine, 5-carboxymethyluridine (cm^5U), into 5-methoxycarbonylmethyluridine (mcm^5U) in a subset of tRNAs (*13*). Human ALKBH8 has also been shown to catalyze the generation of mcm^5U at the wobble position of tRNA and can partially rescue the formation of mcm^5U in *S. cerevisiae* cells lacking Trm9 (*8*, *14*, *15*). These results indicate that ALKBH8 is a functional Trm9 homolog. In contrast to ALKBH8, however, TRM9L is unable to rescue the formation of mcm^5U in Trm9-deficient *S. cerevisiae* cells, and no methyltransferase activity has yet been demonstrated for TRM9L in vitro (*8*). Thus, TRM9L could require additional cofactors for methyltransferase activity or have acquired functions different than canonical Trm9 enzymes.

Here, we demonstrate that TRM9L is a phosphoprotein with phosphorylation playing a key role in its tumor inhibition behavior. Stress-dependent phosphorylation at multiple serine residues was found to increase sensitivity to tumorigenic stresses, control protein-protein interactions, and suppress tumor growth. In particular, hyperphosphorylation of at least one TRM9L serine residue was found to be mediated by the MEK [mitogen-activated protein (MAP) kinase kinase]–ERK (extracellular signal–regulated kinase)–RSK (ribosomal protein S6 kinase) signaling pathway. Our results position TRM9L as a new signaling node linking oxidative stress with a tumor growth suppression phenotype.

RESULTS

TRM9L contains an intrinsically disordered domain that undergoes dynamic phosphorylation

Using multiple protein folding and prediction algorithms, we examined the protein sequence of TRM9L for features that could provide insight into its mechanism of tumor suppression. Intriguingly, TRM9L is predicted to contain an intrinsically disordered region

[1]Department of Biological Engineering, Massachusetts Institute of Technology, Cambridge, MA 02139, USA. [2]Department of Biology, Center for RNA Biology, University of Rochester, Rochester, New York 14627, USA. [3]The RNA Institute and Department of Biological Sciences, University at Albany, State University of New York, NY 12222, USA. [4]Singapore-MIT Alliance for Research and Technology, Singapore 138602, Singapore.
*Corresponding author. Email: pcdedon@mit.edu (P.C.D.); dragonyfu@rochester.edu (D.F.); tbegley@albany.edu (T.J.B.)

embedded within the methyltransferase domain that is distinct in homology from yeast Trm9 and human ALKBH8 (Fig. 1A and figs. S2, A and B) (*16*). Further in silico analysis revealed the presence of >30 predicted kinase phosphorylation motifs located within the disordered domain of TRM9L, with only one predicted phosphorylation motif lying outside this domain (fig. S2, C and D) (*17*). These predictions suggest that TRM9L could play a signaling role in tumor suppression as a phosphoprotein (*18*, *19*).

Previous studies have shown that phospho-signaling pathways involved in tumor suppression are readily activated by loss of anchorage due to cell detachment (*20*–*25*). Thus, we investigated whether the phosphorylation status of TRM9L in human HCT116 + TRM9L colon carcinoma cells was altered by trypsin-induced cell detachment, a standard tissue culture procedure. A rapid mechanical collection method that minimizes signaling changes was used as the control. The HCT116 + TRM9L cell line was constructed by stably transducing the parental HCT116 colorectal carcinoma cell line, in which native *TRM9L* expression is undetectable (*8*), with a retroviral vector carrying FLAG-tagged *TRM9L*. For the mechanical collection method, cells were chilled on ice before scraping. The chilling step was presumed to slow down the activities of intracellular kinases and phosphatases and to help with preservation of basal TRM9L phosphorylation status. To monitor the phosphorylation status of TRM9L, we used a gel mobility shift assay based on the differential electrophoretic migration of phosphorylated proteins during sodium dodecyl sulfate polyacrylamide gel electrophoresis (SDS-PAGE) after treatment with calf intestinal phosphatase (CIP) (*26*). Notably, we found that CIP treatment of lysates prepared from HCT116 cells detached by trypsinization led to an increase in TRM9L mobility, which is consistent with phosphorylation of TRM9L (Fig. 1B, "trypsin"). In contrast, in cells collected by direct mechanical detachment, no major difference in TRM9L mobility was detected in lysates treated with CIP relative to untreated lysates (Fig. 1B, "scraping"). As additional evidence for phosphorylation, we carried out two-dimensional (2D) isoelectric focusing (IEF)/SDS-PAGE to resolve the phosphorylated isoforms of TRM9L based on their isoelectric point (pI) using lysate from cells treated with trypsinization. Using this approach, we also detected the CIP-induced disappearance of multiple low-pI TRM9L isoforms and the appearance of high-pI isoforms, again consistent with removal of phosphates from TRM9L (Fig. 1C). Thus, TRM9L is a phosphoprotein that undergoes inducible phosphorylation to generate multiple phosphorylated isoforms.

To validate and identify the phosphorylated residues, we mapped TRM9L phosphorylation sites by a mass spectrometry (MS)–based phosphoproteomic approach. From lysate of HCT116 + TRM9L cells harvested through trypsinization, TRM9L protein was enriched by anti-FLAG immunoprecipitation and hydrolyzed into peptides by trypsin. Phosphorylated peptides were further enriched by immobilized

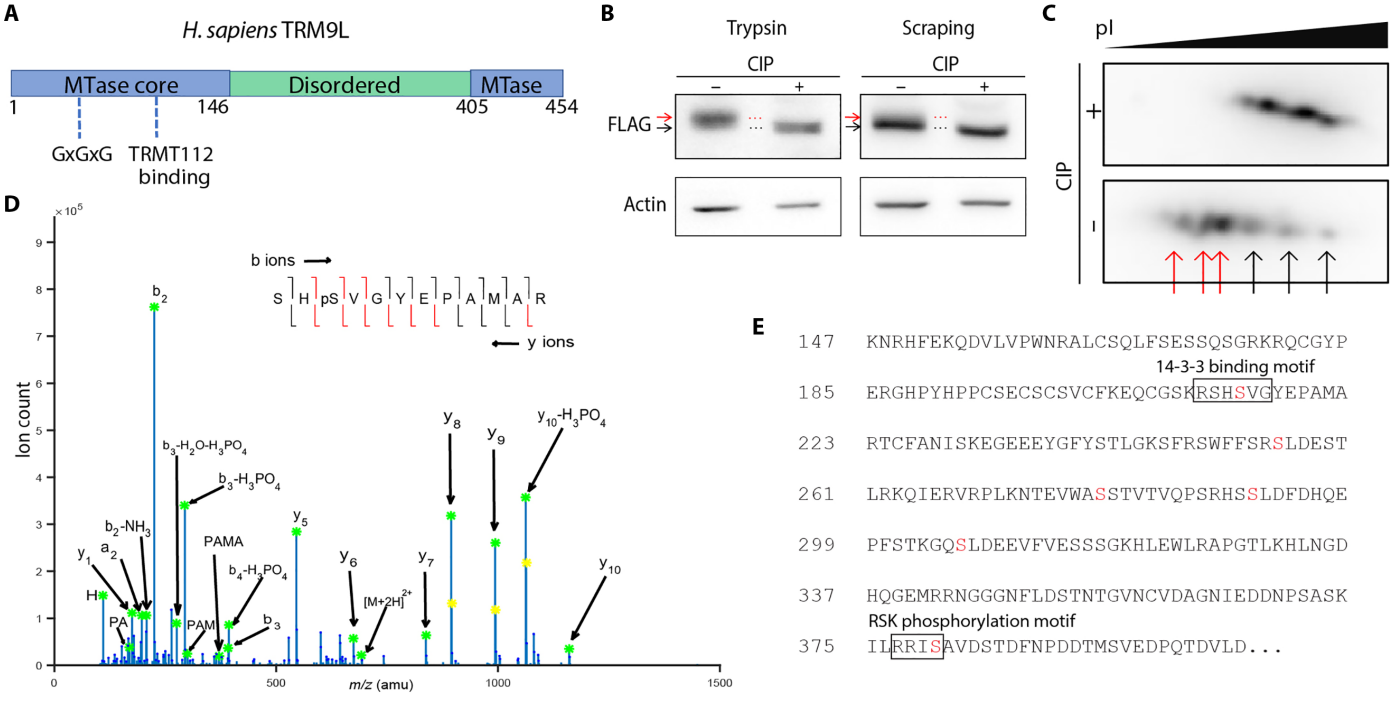

Fig. 1. Phosphorylation of the TRM9L disordered domain. (**A**) Schematic of human TRM9L with conserved N- and C-terminal methyltransferase domains labeled in blue. The nonhomologous internal domain predicted to be an intrinsically disordered is in green. (**B**) Immunoblot analysis of total lysate of HCT116 cells expressing FLAG-TRM9L harvested either by trypsin or mechanical dislodgement (scraping). Lysates were treated without (–) or with (+) CIP. Red and black arrows denote phosphorylated and unphosphorylated forms of TRM9L, respectively. (**C**) Two-dimensional immunoblot analysis of HCT116 cell lysates showing multiple phosphorylation states. Lysates from cells harvested through trypsin were subject to IEF, followed by SDS-PAGE and finally probed by immunoblotting against FLAG-TRM9L. Lysates were treated without (–) or with (+) CIP as in (B). Red and black arrows denote phosphorylated and unphosphorylated forms of TRM9L, respectively. (**D**) Representative MS/MS spectrum of the tryptic TRM9L peptide spanning phosphorylated Ser^{214} (SHpSVGYEPAMAR). b and y ions detected in the MS/MS spectrum were labeled in red. Phosphorylation of Ser^{214} is established by the presence of y_{10}, y_{10}-H_3PO_4, b_3, and b_3-H_3PO_4 ions. (**E**) Primary sequence of the intrinsically disordered domain of TRM9L with phosphorylated residues labeled in red. Sequences consistent with the canonical 14-3-3 binding motif and the RSK phosphorylation motif were boxed. amu, atomic mass unit; *m/z*, mass/charge ratio.

metal affinity chromatography and analyzed by MS. After manual validation of the tandem MS (MS/MS) spectra, six sites of TRM9L phosphorylation were assigned with high confidence, all at serine residues in the disordered domain: Ser^{214}, Ser^{255}, Ser^{279}, Ser^{291}, Ser^{306}, and Ser^{380} (Fig. 1, D and E, and fig. S3). These results demonstrate that TRM9L undergoes phosphorylation on multiple serine residues and suggest a potential role for phosphorylation in the biological function of TRM9L.

Oxidative stress induces the hyperphosphorylation of TRM9L at Ser^{380}

Besides loss of anchorage-dependent growth, oxidative stress constitutes another feature of cancer. Many tumor cells are characterized by elevated levels of reactive oxygen species (ROS) due to the Warburg effect and hypoxia-induced disruption of mitochondrial electron transport (*27*, *28*). On the basis of the critical role of oxidative stress management in tumor growth and metastasis (*29*, *30*), we examined whether oxidative stress could also trigger the phosphorylation of TRM9L.

Using hydrogen peroxide (H_2O_2) as a model for oxidative stress, we observed a H_2O_2-induced shift in TRM9L migration to a lower mobility form in SDS-PAGE, indicative of TRM9L hyperphosphorylation (Fig. 2A). The hyperphosphorylated form of TRM9L, increased in an H_2O_2 dose–dependent manner (Fig. 2A), was detectable at H_2O_2 concentrations below the median lethal dose of ~700 μM (Fig. 2B) and was rapid (<5 min post-H_2O_2) (Fig. 2C). Further 2D gel analysis revealed multiple H_2O_2-dependent phosphorylation states of TRM9L that could be abrogated by CIP treatment (Fig. 2D). Moreover, we found that exposure to menadione, a superoxide generator (*31*), could also increase the cellular phosphorylation of TRM9L (Fig. 2E, top). In contrast, treatment with γ-radiation had no detectable effect on TRM9L phosphorylation (Fig. 2E, bottom). Quantitative phosphoproteomic analysis revealed that HCT116 + TRM9L cells treated with H_2O_2 increased phosphorylation at Ser^{255}

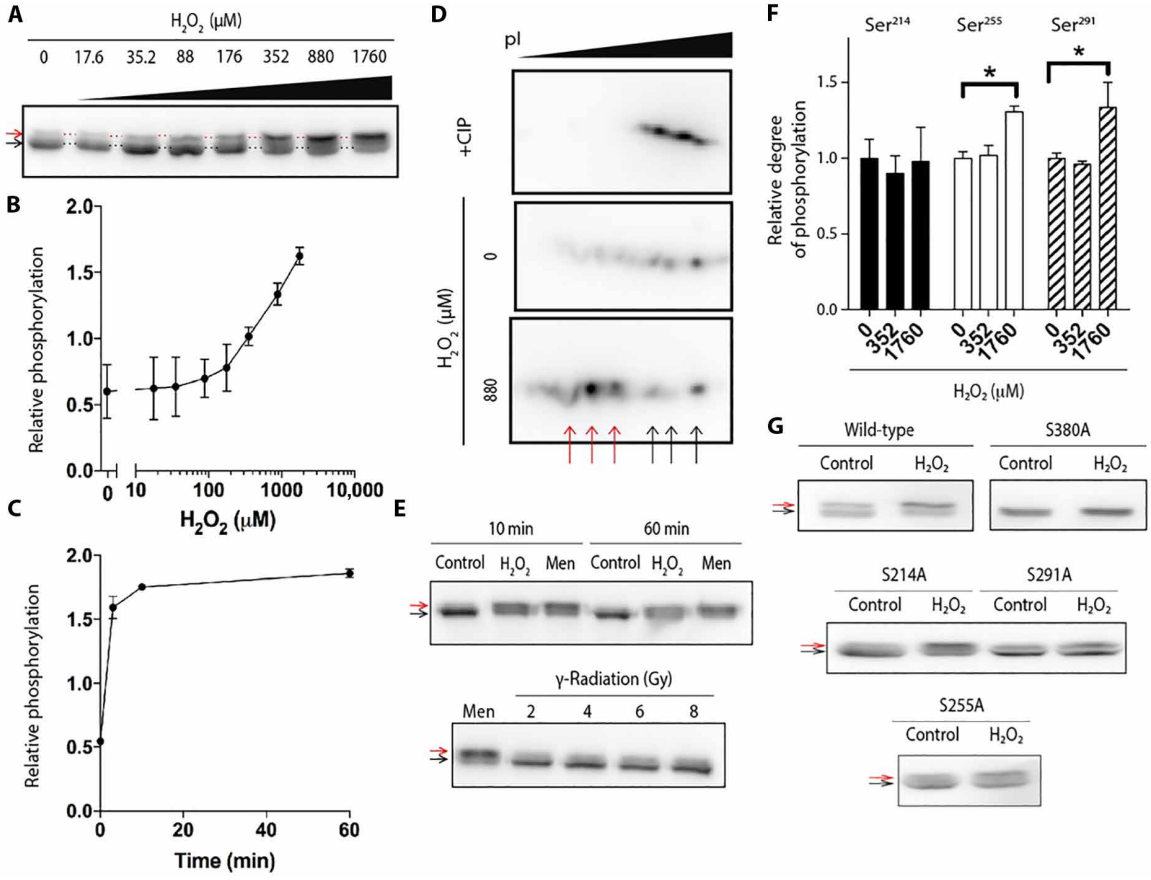

Fig. 2. Oxidative stress induces hyperphosphorylation of TRM9L. (**A**) HCT116 + FLAG-TRM9L cells treated at the indicated concentration of H_2O_2 were harvested by mechanical dislodgement and analyzed by immunoblot for FLAG-TRM9L. (**B**) TRM9L phosphorylation status in HCT116 cells after 10 min of exposure with the indicated dose of H_2O_2. (**C**) Kinetics of TRM9L hyperphosphorylation in HCT116 cells after exposure to 880 μM H_2O_2. For (B) and (C), relative phosphorylation represents the ratio of phosphorylated TRM9L to unphosphorylated TRM9L signal at each time point or dose; data represent means ± SD (n = 3). (**D**) Two-dimensional gel analysis reveals multiple sites of H_2O_2-induced TRM9L phosphorylation. HCT116 + FLAG-TRM9L cells were mock-treated or treated with 880 μM H_2O_2, harvested by mechanical dislodgement, and analyzed by 2D gel. Lysates prepared from cells treated with H_2O_2 were treated without (–) or with (+) CIP. (**E**) Menadione (Men) and H_2O_2, but not γ-radiation, induce TRM9L phosphorylation. HCT116 + FLAG-TRM9L cells were mock-treated or treated with the indicated dose of menadione, H_2O_2, or γ-radiation followed by mechanical harvesting and immunoblot analysis of cell lysates for FLAG-TRM9L. (**F**) Quantitative phosphoproteomic reveals a H_2O_2-induced increase in TRM9L phosphorylation at Ser^{255} (white) and Ser^{291} (hatched) but not Ser^{214} (black) in HCT116 + FLAG-TRM9L cells; data represent means ± SD (n = 3 at each dose of H_2O_2). (**G**) H_2O_2-induced Ser^{380} phosphorylation, but not other sites, determines the 1D gel mobility shift. HCT116 cells expressing the indicated TRM9L variants were mock-treated or exposed to 880 μM H_2O_2 followed by immunoblot analysis of cell lysates for FLAG-TRM9L. Gy, gray.

and Ser^{291} in TRM9L with no significant change in Ser^{214} phosphorylation (Fig. 2F). Phosphorylation at other serine residues could not be confidently quantified because of limitations of the phosphoproteomic method.

To determine which phosphorylation sites contributed to the TRM9L mobility shift observed by SDS-PAGE, we generated serine-to-alanine mutants of TRM9L at residues 214, 255, 291, and 380. These serine residues were chosen because they reside within the consensus sequences of known kinase phosphorylation sites that could be tested using chemical inhibitors. We found that mutation of Ser^{380} abolished the TRM9L gel mobility shift induced by H_2O_2, with no such effect detected for the other mutants (Fig. 2G). Further analysis of purified TRM9L-S380A mutant protein from H_2O_2-treated cells via MS revealed that phosphorylation of Ser^{214}, Ser^{255}, Ser^{291}, and Ser^{306} was still detected even though position 380 was unable to be phosphorylated (fig. S4). These results indicate that the H_2O_2-induced low-mobility form of TRM9L apparent by SDS-PAGE resulted from H_2O_2-induced phosphorylation of Ser^{380}. Thus, the relative mobility shift of TRM9L in SDS-PAGE reflects the degree of Ser^{380} phosphorylation. Together, our results uncover an oxidative stress–induced phospho-signaling pathway that triggers the phosphorylation of multiple serines within TRM9L, including a major TRM9L isoform generated by hyperphosphorylation of Ser^{380}.

Hyperphosphorylation of TRM9L Ser^{380} is dependent on activation of the ERK-RSK signaling pathway

ROS leads to the activation of several intracellular signaling networks that are required for maintaining ROS homeostasis and cellular proliferation (*32*, *33*). To decipher the signaling pathways that modulate phosphorylation of TRM9L, we used a chemical genetic approach based on a panel of kinase inhibitors to look for molecules that could inhibit formation of the low-mobility hyperphosphorylated form of TRM9L in SDS-PAGE (table S1). We found that H_2O_2-induced hyperphosphorylation of TRM9L Ser^{380} was diminished in cells pretreated with inhibitors of the MAP kinase kinase MEK1 and MEK2 (table S1, U0126 and PD98059). Although commonly thought to be downstream of growth factors, ERKs have been reported to be activated by oxidative stress; for instance, oxidative stress including H_2O_2 can activate membrane-associated receptor tyrosine kinases, such as the epidermal growth factor receptor (EGFR), to initiate the ERK signaling cascade (Fig. 3A) (*34*–*36*). We confirmed that H_2O_2 can induce the activation of the ERK signaling pathway in HCT116 + TRM9L cells based on H_2O_2-induced Thr^{202}/Tyr^{204} dual phosphorylation of ERK1/2 (p-ERK1/2) (Fig. 3B, +H_2O_2). Moreover, we validated that preincubation with the MEK1/2 inhibitor U0126 abolished the H_2O_2-induced phosphorylation of ERK1/2 and the hyperphosphorylation of TRM9L Ser^{380} (Fig. 3B, +H_2O_2 and +U0126). In contrast to inhibitors of the ERK signaling pathway, no major effect on TRM9L hyperphosphorylation was detected for the other kinase inhibitors, including inhibitors of the related MAP kinases, p38, and c-Jun N-terminal kinase (table S1). These results support the idea that oxidative stress–induced hyperphosphorylation of TRM9L is primarily dependent on activation of the MEK-ERK signaling pathway.

As a major transducer of the ERK signaling pathway, RSK phosphorylates numerous downstream targets, including those that activate the oxidative stress response (Fig. 3A) (*37*, *38*). Among the TRM9L phosphorylation sites confirmed here, we found that Ser^{380} lies within a consensus motif (RRIpS) for RSK phosphorylation (Fig. 1E) (*39*). To test the role of RSK in hyperphosphorylation of TRM9L Ser^{380}, we inhibited all four isoforms of RSK using the cell permeable inhibitor BI-D1870 and found that RSK inhibition can indeed decrease H_2O_2-induced hyperphosphorylation of TRM9L Ser^{380} (Fig. 3C). A similar inhibition of H_2O_2-induced hyperphosphorylation of TRM9L Ser^{380} was also observed for a different compound, AZD7762, which was initially developed as a CHEK1/2 inhibitor

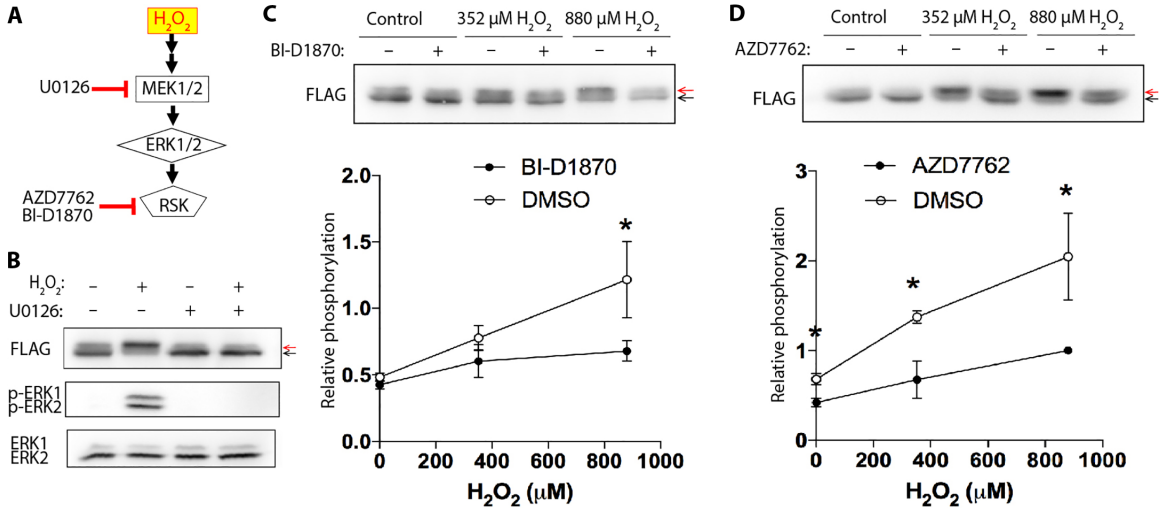

Fig. 3. H_2O_2-induced hyperphosphorylation of TRM9L is dependent on the ERK- and RSK-signaling pathways. (**A**) Simplified schematic of the MEK/ERK signaling pathways transduced through RSK. Kinase inhibitors used in this study are denoted. (**B**) H_2O_2-induced Thr^{202}/Tyr^{204} dual phosphorylation of ERK1/2 and hyperphosphorylation of TRM9L are dependent on MEK1/2 activation. HCT116 + FLAG-TRM9L cells that were untreated or exposed to 880 μM H_2O_2 with or without the pretreatment of MEK1/2 inhibitor U0126 were harvested by mechanical dislodgement and analyzed by immunoblot for the indicated proteins. (**C** and **D**) H_2O_2-induced hyperphosphorylation of TRM9L is inhibited by pretreatment of the RSK inhibitors BI-D1870 (C) and AZD7762 (D). Top: HCT116 + FLAG-TRM9L cells were left untreated or treated with the indicated concentration of H_2O_2 in the presence of vehicle [dimethyl sulfoxide (DMSO)] or the indicated RSK inhibitor followed by immunoblot analysis. Bottom: Quantification of H_2O_2-induced hyperphosphorylation of Ser^{380} in the presence of DMSO or RSK inhibitor. Data represent means ± SD (n = 3).

but was later found to be a potent inhibitor of RSK2 and RSK3 as well (Fig. 3D) (*40*). Collectively, these findings reveal TRM9L as a phosphorylation target downstream of the MEK-ERK-RSK signaling pathway in response to oxidative stress.

TRM9L interacts with 14-3-3 signaling proteins in a phosphorylation-dependent manner

The H_2O_2-induced phosphorylation of TRM9L could promote protein-protein interactions with further downstream effectors to carry out the tumor inhibition role of TRM9L. To identify TRM9L-interacting proteins, we transiently expressed and affinity-purified TRM9L from human embryonic kidney (HEK) 293T cells detached by trypsin, followed by analysis of associated proteins. The HEK 293T cell line was chosen as it was able to achieve a high expression level of TRM9L via transient transfection. As a control study, we also purified ALKBH8, a paralog of TRM9L (*14*). Silver stain analysis of the eluted fractions revealed the presence of several bands at ~28 kDa specifically in the TRM9L pulldown, but not with vector control or ALKBH8 (Fig. 4A). MS analysis of the gel-excised 28-kDa bands revealed the presence of the 14-3-3 family of signaling proteins (Fig. 4B). To ensure that the copurification of 14-3-3 proteins was not simply due to overexpression, we also investigated the interaction of 14-3-3 proteins with TRM9L expressed at lower levels in a stable 293T cell line. Analysis of copurifying proteins by silver stain and by liquid chromatography (LC)–MS also revealed the copurification of 14-3-3 proteins with stably expressed TRM9L (Fig. 4, C and D). We note that the increased background of contaminants was due to the much longer exposure time necessary to develop the silver stain to visualize the lower levels of TRM9L purified from stable cell lines.

Since the primary sequence of 14-3-3 proteins contains a high degree of identity to each other and cannot be easily distinguished by MS, we validated the identity of each 14-3-3 protein using immunoblotting with antibodies specific to each 14-3-3 protein. Here, we detected the specific copurification of 14-3-3 gamma, epsilon, and eta with TRM9L, while no signal was detected for the other 14-3-3 proteins (Fig. 4E). The 14-3-3 family of signaling proteins, via binding to target motifs containing phospho-serine or phospho-threonine, are well-known regulators of proteins phosphorylated by RSK (*41*–*43*). Moreover, 14-3-3 proteins form homo- or heterodimers that interact with phosphorylated serine/threonine residues of client proteins (*44*). Notably, the phosphorylated Ser^{214} site of TRM9L lies within a canonical 14-3-3 binding motif (RSHpSVG), while Ser^{255} is a partial match for a consensus 14-3-3 binding motif (Fig. 1E) (*45*). Using the TRM9L serine-to-alanine mutants described above, we found that mutation of either Ser^{214} or Ser^{255} abrogated binding of all 14-3-3 proteins to TRM9L as detected by immunoblotting (Fig. 4E). In contrast, mutation of either Ser^{380} or Ser^{291} had no effect on 14-3-3 binding to TRM9L (Fig. 4F). The interaction of 14-3-3 gamma, epsilon, and eta with TRM9L that are dependent on either Ser^{214} or Ser^{255} was also confirmed using a completely different affinity purification approach with the FLAG tag system (fig. S5). Since we were interested in the potential role that TRM9L-14-3-3 interaction may play in the tumor inhibition activity of TRM9L, we also investigated the interaction between 14-3-3 proteins and TRM9L in the SW620 colorectal cancer cells. Using SW620 cells stably expressing TRM9L, we were also able to show that 14-3-3 proteins interact with TRM9L (Fig. 4G). Furthermore, we were able to show that TRM9L expression sensitizes SW620 cells to the 14-3-3 antagonist BV02, leading to decreased viability in cell culture (fig. S6). Altogether, our results identify 14-3-3 proteins as interacting partners of TRM9L, with binding dependent on the phosphorylation of serine residues Ser^{214} and Ser^{255} in TRM9L.

TRM9L phosphorylation is required for oxidative stress hypersensitization and tumor suppression

Given the critical roles played by 14-3-3 proteins (*45*) and MEK-ERK-RSK signaling (*46*) in modulating cell cycle progression and apoptosis in response to developmental and environmental cues, the results to this point suggest a key role for TRM9L phosphorylation in controlling cell fate in response to tumorigenic conditions. To test the cellular function of TRM9L phosphorylation, we quantified the effect of TRM9L on oxidative stress survival in two types of colorectal carcinoma cells with distinct origins, HCT116 and SW620. In both cell lines, expression of native *TRM9L* is undetectable (*8*). We found that re-expression of TRM9L in either human HCT116 or SW620 colon carcinoma cells leads to increased sensitivity to oxidative stress induced by H_2O_2 (Fig. 5, A and C). In contrast, TRM9L expression had no effect on cellular sensitivity to ionizing radiation (Fig. 5, B and D), consistent with the lack of TRM9L hyperphosphorylation induced by γ-radiation (Fig. 2E, bottom). In addition, H_2O_2 treatment of HCT116 + TRM9L cells pretreated with an RSK inhibitor, AZD7762, resulted in increased survival compared to HCT116 + TRM9L cells treated with H_2O_2 alone (Fig. 5E), whereas the AZD7762 pretreatment did not cause significant difference in the survival of HCT116 + LacZ cells treated with H_2O_2 (Fig. 5F). This suggested that the increase in the survival of HCT116 + TRM9L cells mediated by AZD7762 was due to its effect on TRM9L protein and not due to other effects that the molecule might have on the cell. Thus, re-expression of TRM9L in colorectal cancer cells leads to oxidative stress hypersensitization, with TRM9L phosphorylation playing a key role in determining cell survival.

Finally, we tested whether the phosphorylation of TRM9L plays a role in tumor suppression using an in vivo xenograft model based on the chicken chorioallantoic membrane (CAM) tumor formation assay (*47*). We tested the tumor-forming potential of SW620 colon cells expressing either LacZ, wild-type (WT) TRM9L, or the TRM9L mutants S214A, S255A, S291A, and S380A. The SW620 cell line was chosen for its ability to form a solid tumor in the CAM model (*48*). All TRM9L mutants were found to express at or above the level of WT in the cells used for this assay (fig. S7). Confirming our previous results (*8*), re-expression of WT TRM9L could greatly suppress SW620 tumor cell growth relative to control SW620 cells expressing LacZ alone (Fig. 5G). Strikingly, the TRM9L mutants S214A, S255A, and S380A were greatly impaired for tumor growth suppressor activity relative to WT TRM9L (Fig. 5G). In contrast, mutation of Ser^{291} had no effect on the tumor suppressor activity of TRM9L, consistent with the lack of a detectable function for that particular phosphorylated residue. Altogether, these findings unveil a pivotal role for TRM9L hyperphosphorylation in determining cancer cell survival and tumor growth suppression through the activation of the MEK-ERK-RSK signaling pathway.

DISCUSSION

Here, we show that TRM9L is phosphorylated at multiple serine residues and that certain types of oxidative stress induce the hyperphosphorylation of TRM9L. Furthermore, we provide evidence that the effect of TRM9L on cell proliferation is mediated by ROS-dependent

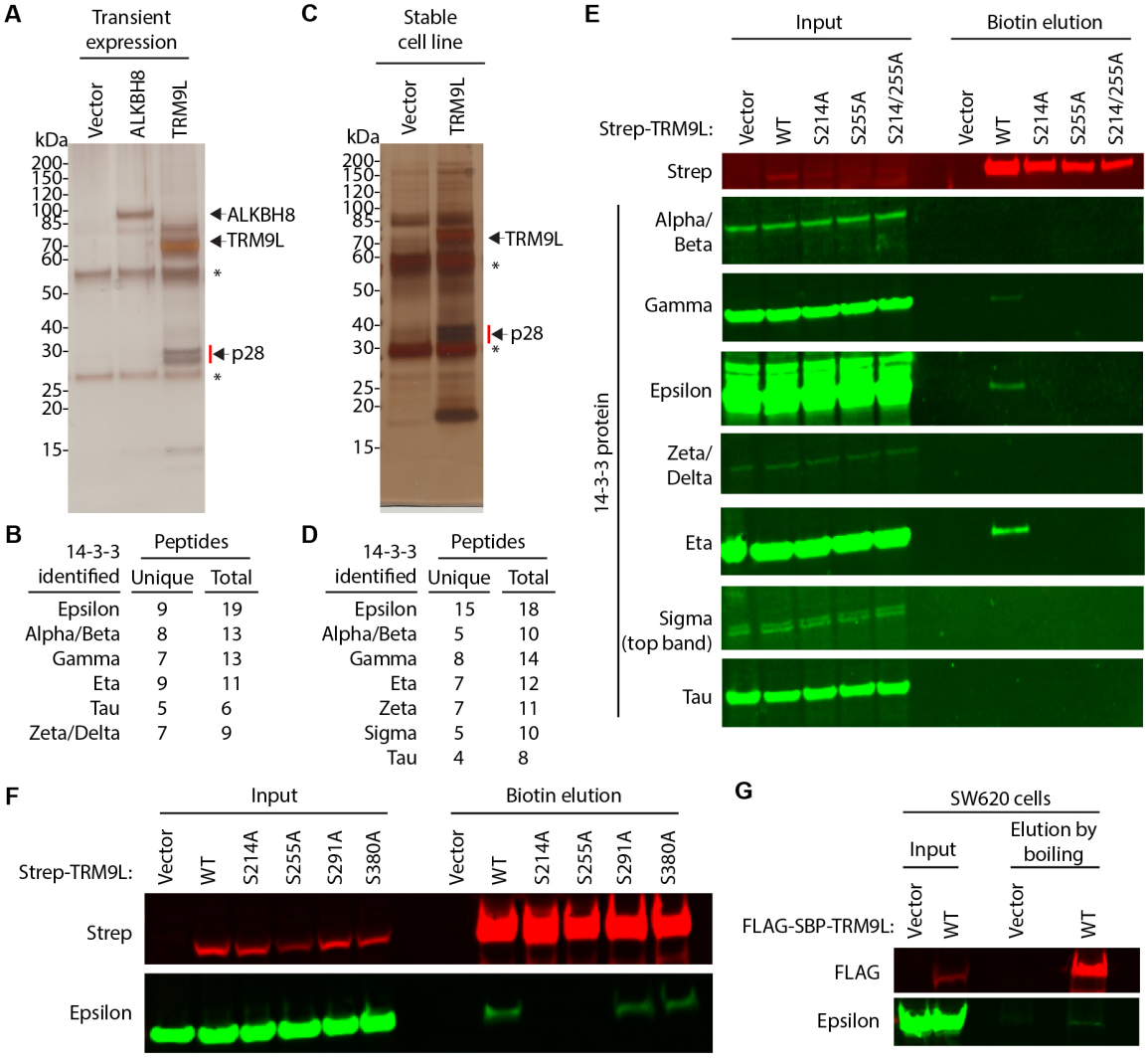

Fig. 4. Phosphorylation-dependent interaction of TRM9L with 14-3-3 proteins. (**A**) Silver stain of FLAG-SBP–tagged ALKBH8 or TRM9L affinity-purified from transiently transfected HEK 293T cells. Arrows point to bait proteins, while p28 indicates copurifying proteins processed for LC-MS peptide identification. "*" denotes antibody heavy/light chain from acid elution. (**B**) LC-MS identification of proteins in the p28 gel band. The 14-3-3 proteins that were identified, number of unique peptides, and total number of peptides from the p28 gel slice are noted. (**C**) Silver stain of FLAG affinity purifications from extracts prepared from HEK 293T cells stably expressing either empty vector or FLAG-SBP-TRM9L. Arrow points to bait protein, while p28 represents copurifying proteins processed for LC-MS protein identification. "*" is antibody heavy/light chain from acid elution. (**D**) LC-MS identification of proteins present in total elutions from purifications in (C). All 14-3-3 proteins that were identified are noted with the number of unique peptides and total number of peptides. (**E**) Immunoblot verification of 14-3-3 proteins copurifying with Strep-tagged TRM9L variants transiently expressed in HEK 293T cells. Strep-TRM9L-WT copurifies biotin elution with 14-3-3 gamma, epsilon, and eta, while TRM9L S214A and S255A lacked copurification of 14-3-3 proteins. "Input" represents 2% of total protein extract, while biotin elution represents 15% of total purification. (**F**) Immunoblot showing that all, while "biotin elution" represents 30% of total purification. TRM9L variants except S214A and S255A copurify with 14-3-3 epsilon when transiently expressed in HEK 293T cells. "Input" represents 4% of total protein extract , while "biotin elution" represents 30% of total purification. (**G**) Immunoblot verification of 14-3-3 copurification with TRM9L from SW620 cells. One hundred percent of elutions from FLAG affinity purifications from SW620 cells stably expressing FLAG-SBP-TRM9L were loaded. For "input," 4% of starting input extracts were loaded.

phosphorylation linked to ERK-RSK signaling and 14-3-3 binding. Collectively, our studies establish that the tumor growth suppressing activity of TRM9L is dependent on at least three of six phosphorylation sites linked to these pathways. These results support a model in which an ERK/RSK-dependent phospho-signaling regulatory mechanism underlies the tumor-inhibiting behavior of TRM9L, with oxidative stress capable of activating the regulatory pathway (Fig. 6).

The activation of ERK by H_2O_2 cannot be overlooked, given the central role of ERK as a proto-oncogene and the association of mutations in EGFR-Ras-Raf-MEK-ERK pathway components with tumorigenesis and metastasis (*49*), as well as the central role of ROS in tumorigenic inflammation (*50*) and the hypoxic tumor microenvironment (*27*). Previous studies have demonstrated H_2O_2 activation of ERK1 in hepatocytes, with functional distinctions between EGFR- and ROS-induced ERK activation (*38*). Studies in H_2O_2-treated glioma cells further revealed ERK-dependent RSK activation (*51*). While further work is needed to delineate the molecular mechanism, our studies provide a contextual link between ROS, the ERK-RSK pathway, TRM9L phosphorylation–dependent 14-3-3 binding, and tumor growth suppression. This is consistent with the observation

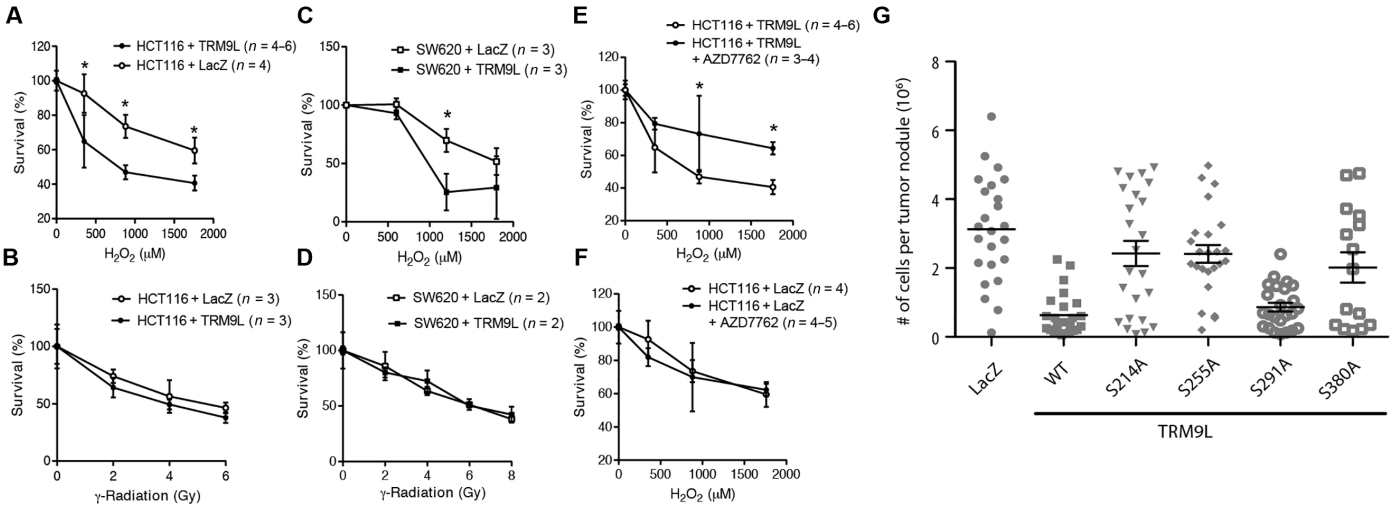

Fig. 5. Multiple TRM9L phosphorylation sites link ROS signaling and tumor growth suppression. (**A** to **D**) TRM9L re-expression sensitizes colon cancer cell lines to oxidative stress but not γ-radiation. Survival of the indicated human cell lines 24 hours after treatment with H_2O_2 or ionizing radiation was measured by trypan blue staining. Data represent means ± SD, and asterisks denote significance ($P \leq 0.05$) in a Student's *t* test. (**E** and **F**) Sensitization of colon cancer cell lines by TRM9L re-expression to H_2O_2 is dependent on MEK-ERK signaling. Survival of the indicated human cell lines 24 hours after treatment with H_2O_2 with or without the pretreatment of the RSK inhibitor was measured as in (A) to (D). (**G**) Tumor growth suppression is dependent on TRM9L hyperphosphorylation. Xenografts of SW620 cell lines expressing the indicated TRM9L variants or LacZ (as a negative control) were implanted onto chick CAMs followed by analysis of tumor cell growth. Relative to WT TRM9L–expressing cells, tumor growth (CAM xenografts) is suppressed by phosphorylation at Ser^{214} ($P < 0.0007$), Ser^{255} ($P < 0.0001$), and Ser^{380} ($P < 0.01$). Bars represent means ± SD for the data representing individual tumor samples, with a Mann-Whitney test for significance.

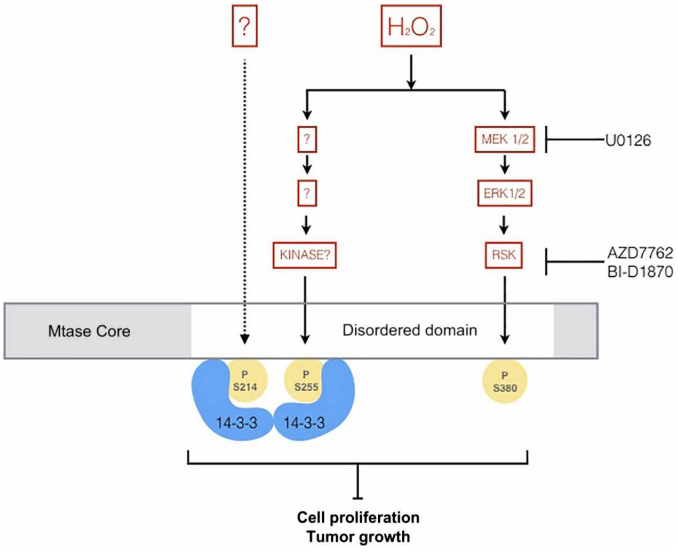

Fig. 6. Phosphorylation of human TRM9L is a critical regulator of oxidative stress survival and tumor growth suppression. Oxidative stress conditions induce TRM9L hyperphosphorylation through the MEK-RSK signaling pathway. Hyperphosphorylation of TRM9L inhibits cell proliferation and suppresses tumor cell growth.

that TRM9L expression promotes cellular senescence and sensitivity to hypoxia as well as ROS (*8*), with phospho-signaling now added as a modulator of TRM9L activity.

Another major consequence of TRM9L phosphorylation involves putative conformational changes controlling protein-protein interactions. The intrinsically disordered domain of TRM9L, which is absent in yeast Trm9 and human ALKBH8, is host to >30 kinase recognition and protein-binding motifs (fig. S2C). Emerging evidence points to disordered domains as critical features of many signaling and regulatory proteins, with phosphorylation and protein-protein interactions stabilizing and organizing the domains for functional activity (*18*, *19*). Of these 30 sites, we demonstrated functional activity for three serine residues in RSK phosphorylation and 14-3-3 binding. Through mutagenesis studies, we found that 14-3-3 binding depends on phosphorylation of both Ser^{214} positioned in a 14-3-3 binding motif and the Ser^{255} site lying in a partial 14-3-3 consensus motif (Fig. 4E), with only Ser^{255} phosphorylation between the two sites increasing during oxidative stress (Fig. 2F). This raises the possibility that 14-3-3 binding to TRM9L increases during oxidative stress as part of the H_2O_2-activated ERK/RSK pathway. Considering that chaperone-like stabilization of binding partners is one of the many functions of 14-3-3 proteins (*45*), the binding of 14-3-3 proteins could further stabilize the intrinsically disordered domain of TRM9L to facilitate an active conformation.

Finally, a surprising feature of TRM9L is its hyperphosphorylation induced by H_2O_2 but not by ionizing radiation, at least for Ser^{380}. The observation that TRM9L expression sensitizes cells to H_2O_2 exposure (Fig. 5, A and C) is consistent with our previous observation that TRM9L promotes senescence and increases hypoxia sensitivity to suppress tumor growth (*8*). However, the lack of an effect of TRM9L on ionizing radiation–induced cytotoxicity points to very different chemical mechanisms underlying H_2O_2 and ionizing radiation stress. Both agents can form hydroxyl radical (HO•), but this reaction requires a redox-active metal for H_2O_2, which localizes the damage to within 100 Å of the metal due to the high reactivity of HO• (*50*). On the other hand, the HO• and other radical species produced along the essentially random cellular tracks of photons during γ-radiation are not targeted (*52*, *53*). Differences between H_2O_2 and ionizing radiation are also apparent at the level of transcriptional

activation and repression in human cells (*54*, *55*). Along with the well-established signaling function of H_2O_2 by virtue of selective oxidation of cysteines in signaling proteins (*56*), these differences may explain how the signaling pathways that lead to hyperphosphorylation of TRM9L, including the MEK-ERK-RSK pathway, differentiate between H_2O_2 and ionizing radiation in TRM9L's decision-making function to influence cell survival and promote senescence. Future studies will be devoted to understanding this distinction at a molecular and atomic level.

MATERIALS AND METHODS

Primary sequence analysis

The primary amino acid sequence corresponding to UniProt #Q9P272-1 was used for all in silico analyses. Prediction of phosphorylation sites was made by entering the primary amino acid sequence into DISPHOS 1.3 (www.dabi.temple.edu/disphos/) with setting on "default predictor". For the same purpose, the PHOSIDA predictor for phosphorylation in *Homo sapiens* (http://141.61.102.18/phosida/index.aspx, select "tools" tab) was also used. Prediction intrinsic disorder in protein structure was made by entering the primary amino acid sequence into FoldIndex (https://fold.weizmann.ac.il/fldbin/findex) with the following settings: window = 51 and step = 1.

Reagents

Unless otherwise stated, reagents were of American Chemical Society (ACS) reagent grade or better (Sigma-Aldrich). Antibodies included: anti-FLAG M2 and goat anti-mouse horseradish peroxidase (HRP) (Sigma-Aldrich); anti–β-actin (13E5), anti–phospho-ERK1/2 (Thr^{202}/Tyr^{204}), anti-ERK1/2, anti-RSK2, anti–poly(ADP-ribose) polymerase 1, and the anti–14-3-3 Alpha/Beta, Gamma, Delta/Zeta, Eta, Tau 14-3-3 Family Antibody Sampler Kit (Cell Signaling Technology); monoclonal anti-Streptag II (Thermo Fisher Scientific); anti-TRMT112 (F-7), anti–14-3-3 Epsilon (T-16), goat anti-rabbit HRP (Santa Cruz Biotechnology); anti–14-3-3 Sigma (Bethyl Laboratories); goat anti-rabbit 800 (Thermo Fisher Scientific); and goat anti-mouse 680 (LI-COR Biosciences).

Cell line construction

HCT116 and SW620 cells expressing LacZ or FLAG-tagged TRM9L were prepared as described previously (*8*). The FLAG-tagged TRM9L coding sequence contains three naturally occurring single-nucleotide polymorphisms that differ from the SwissProt (www.uniprot.org) reference sequence: H150R, C207G, and G304E. Cell lines were maintained in Dulbecco's minimal essential medium (DMEM) [glucose (4.5 g/liter), glutamine-free, Lonza] supplemented with 10% fetal bovine serum (FBS) (Atlantic Biologicals), penicillin (100 U/ml) with streptomycin (100 μg/ml) (pen/strep, Lonza), and 2 mM glutamine (Lonza) in humidified 5% CO_2 at 37°C. For TRM9L point mutants, site-directed mutagenesis was performed using polymerase chain reaction (PCR)–based approaches and verified by DNA sequencing. DNA primers were designed to replace the appropriate bases in the coding sequence of TRM9L: serine (AGT) to alanine (GCC) at position 214 (S214A mutant), serine (TCT) to alanine (GCT) at position 255 (S255A mutant), serine (AGT) to alanine (GCT) at position 291 (S291A mutant), and serine (TGT) to alanine (GCA) at position 380 (S380A mutant). Stable SW620 and HCT116 cells expressing TRM9L mutant constructs were made by retroviral transduction as described previously (*8*). The HEK 293T and derivative cell lines were cultured in DMEM containing 10% FBS (Thermo Fisher Scientific), 2 mM L-alanyl-L-glutamine (GlutaMAX, Gibco), and 1% penicillin/streptomycin (Gibco).

Treatment with oxidants

Cells (1×10^6) were seeded in six-well plates and covered with medium (2 ml). After overnight incubation at 37°C, medium was aspirated, washed once with phosphate-buffered saline (PBS) (tissue-culture grade, Lonza), and covered with 2 ml of ambient-temperature FBS-free medium, followed by addition of oxidants (H_2O_2 diluted in PBS, menadione diluted in DMSO, or PBS alone as a control). The plate was immediately incubated at 37°C. At various times, medium was aspirated, and cells were washed with PBS before proceeding to lysis.

Kinase inhibitor treatments

Cells (1×10^6) were seeded in six-well plates and covered with medium (2 ml). After overnight incubation, kinase inhibitors diluted in DMSO were added: U0126 (10 μM), a selective MEK1/2 inhibitor (Cell Signaling Technology); AZD7762 (150 nM), a selective inhibitor of checkpoint kinases 1 (Chk1) and Chk2, which also inhibits RSK2/3 (Cayman Chemicals); and BI-D1870 (10 μM), a potent inhibitor of the N-terminal kinase domain of RSK 1, 2, 3, and 4 (Cayman Chemicals). Cells were incubated at 37°C for an additional 75 min and then treated with oxidants as described above. Kinase inhibitors were also added in the FBS-free medium used for H_2O_2 treatment.

Survival measurement

After cells were treated with oxidants as described above or irradiated with the desired dose of ^{137}Cs γ-radiation, they were washed with PBS once and replenished with fresh medium. Cells were continuously incubated for 24 hours before being trypsinized. The number of surviving cells was determined by resistance to trypan blue staining. For each cell line, the number of surviving cells in each treatment condition was compared against that in the untreated control sample to obtain the percentage survival. Statistical significance was determined by a Student's *t* test at each dose of treatment.

Cell lysate preparation

Unless otherwise stated, cells were detached from tissue culture plates by trypsinization (0.05% trypsin-EDTA without Ca^{2+}/Mg^{2+}, Lonza) at 37°C and collected by centrifugation (500*g*, 5 min, 4°C). After aspirating medium, the cell pellet was resuspended in lysis buffer consisting of PBS, 1% Triton X-100, 2 mM EDTA, 1:100 mammalian cell protease inhibitors (Sigma-Aldrich), and 1:100 phosphatase inhibitor (Halt, Thermo Fisher Scientific). Cells were lysed by incubation on ice for 20 min, followed by pipetting to further disrupt the cells. The lysate was cleared by centrifugation (5000*g*, 10 min, 4°C).

For studies with H_2O_2 or menadione, cells were washed once with PBS after treatment, covered with PBS, and immediately placed on ice for 10 min. They were then mechanically dislodged from plates using a cell scraper and collected by centrifugation (500*g*, 5 min, 4°C). Whole-cell lysates were prepared as described above.

Dephosphorylation reactions

Cell lysates (~100 μg of total protein) prepared in the absence of phosphatase inhibitor were diluted with CIP reaction buffer consisting of 50 mM tris-HCl (pH 7.9), 5 mM $MgCl_2$, 0.1 mM dithiothreitol (DTT), and 1:100 protease inhibitor (Sigma-Aldrich) to a total volume of 150 μl. CIP (15 μl, 150 units, New England Biolabs) was then added, and the reaction mixture was incubated at 30°C for 15 min.

The reaction was terminated by addition of Laemmli buffer (Bio-Rad Laboratories) for SDS-PAGE or by adding a 6× volume of ice-cold acetone for 2D gel analysis.

One-dimensional SDS-PAGE Western blots

Cell lysate was mixed with 4× Laemmli buffer (3:1) and heated at 95°C for 5 min before loading onto a 1.5-mm-thick 8% acrylamide gel [bisacrylamide/acrylamide = 1:37.5, 375 mM tris-HCl (pH 8.8), 0.1% (w/v) SDS, 0.1% (w/v) ammonium persulfate (APS), and 0.01% (v/v) tetramethylethylenediamine (TEMED)], with a 4% acrylamide stacking layer [bisacrylamide/acrylamide = 1:37.5, 125 mM tris-HCl (pH 6.8), 0.1% (w/v) SDS, 0.1% (w/v) APS, and 0.01% (v/v) TEMED] poured in Bio-Rad Mini-PROTEAN short plates and left at ambient temperature overnight before use. After loading, the gel was run in a Bio-Rad Mini-PROTEAN III electrophoresis system at 150 V for 1 hour, followed by electrotransfer to polyvinylidene difluoride (PVDF) membrane (0.2-μm pore, Bio-Rad Laboratories) using the standard tank transfer method at 300 mA for 1 hour. The PVDF membrane was then blocked with 3% milk at room temperature for 30 min, probed by the primary antibody at 4°C overnight and secondary antibody at room temperature for 1 hour, and finally visualized using enhanced chemiluminesence (SuperSignal West Dura, Thermo Fisher Scientific) and a charge-coupled device camera (FluorChem 8900, Alpha Innotech). The degree of phosphorylation was calculated as the ratio of the intensity of the slower band to that of the faster band. Each data point represents the mean ± SD for three biological replicates. Samples were compared using an unpaired Student's *t* test ($P < 0.05$).

Two-dimensional IEF–SDS-PAGE Western blots

Ice-cold acetone was added to cleared cell lysate (~100 μg of total protein) at 6:1 v/v, and the mixture was stored at −20°C overnight to precipitate proteins. The suspension was centrifuged (16,000*g*, 20 min, 4°C), and the resulting pellet was washed with ice-cold 80% acetone and air-dried to remove acetone. The pellet was fully dissolved in 125-μl immobilized pH gradient (IPG) dissolution buffer [7 M urea, 2 M thiourea, 1% (w/v) DTT, 5% glycerol, and 1% IPG solution (pH 4 to 7, GE Amersham)], and the solution was loaded evenly onto a 70-mm IPG strip (pH 4 to 7, GE Amersham). IEF was performed on an Agilent 3100 OFFGEL Fractionator (Agilent Technologies) with the following settings: 8 kV· hour, maximum current = 50 μA, maximum voltage = 4500 V, 4°C. After the desired run time was reached, the IPG strip was removed from the fractionator and soaked in 10 ml of equilibration buffer [6 M urea, 2% (w/v) SDS, 50 mM tris-HCl (pH 8.8), 20% glycerol, 1% (w/v) DTT, and bromophenol blue] for 10 min at ambient temperature. It was then positioned atop a 1.5-mm 8% acrylamide gel and encased in molten agar (1% agarose in 1× tris-glycine running buffer). Following agar solidification, the gel (second dimension) was run, and the multiple isoforms of TRM9L were eventually visualized in Western blot, as described above.

MS-based phosphoproteomics

Studies were initiated by immunoprecipitation of TRM9L. Protein G magnetic beads (New England Biolabs) were covalently cross-linked to anti-FLAG M2 using the dimethyl pimelimidate procedure (www.neb.com/protocols/1/01/01/cross-linking-of-igg-to-protein-a-or-g-beads). Whole-cell lysates from treated and untreated HCT116 cells stably expressing TRM9L were diluted with cold lysis buffer to a volume of 300 μl [protein (~3 μg/μl)]. Antibody-linked protein G beads (15 μl) were added, and the mixture was shaken gently at 4°C overnight. The next morning, the depleted lysate was aspirated, and the magnetic beads were washed four times with 800 μl of cold PBS. Antibody-bound proteins were eluted once with 40 μl and twice with 20 μl of 6 M urea at ambient temperature for 10 min.

Proteins in the 6 M urea eluate were reduced (10 mM DTT; 56°C, 45 min) and alkylated (50 mM iodoacetamide; ambient temperature, dark, 1 hour) and subsequently digested with 2.5 μg of trypsin (sequencing grade, Promega; ambient temperature overnight, 100 mM ammonium acetate (pH 8.9)]. Following trypsin quenching with formic acid (5%), peptides were desalted using C18 SpinTips (Protea), lyophilized, and stored at −80°C.

Peptides were labeled with tandem mass tag (TMT) 10plex (Thermo Fisher Scientific) by dissolving lyophilized samples in 70 μl of ethanol and 30 μl of 500 mM triethylammonium bicarbonate (pH 8.5), and then adding the TMT reagent in 30 μl of anhydrous acetonitrile. The solution was vortexed and incubated at ambient temperature for 1 hour. Labeled samples were combined and concentrated in a vacuum centrifuge.

Phosphorylated peptides were enriched using a modification of a published Fe–nitrilotriacetic acid (NTA) affinity purification protocol (*57*). Briefly, following nickel removal from Ni-NTA agarose (Qiagen) with 100 mM EDTA, 100 mM $FeCl_3$ was added to generate Fe-NTA. Acidified peptides were then added and incubated for 1 hour at ambient temperature. Phosphopeptides were eluted with 250 mM sodium phosphate. The flow-through of total peptides was also collected.

For LC-MS/MS analysis, reversed-phase high-performance LC was performed using an in-house generated precolumn (6 cm) packed with C18 (10-μm particle size) and a self-packed 12-cm, 10-μm-tip analytical column (New Objective) packed with C18 (5-μm particle size), mounted in an EASY- nLC1000 (Thermo Fisher Scientific), and eluted with a 70-min gradient (200 nl/min) for enriched phosphopeptides and a 140-min gradient for flow-through total peptides. The eluent was directed into a nanoelectrospray ionization-mode QExactive Plus mass spectrometer (Thermo Fisher Scientific). The mass spectrometer was operated in a data-dependent mode with the following parameters for the full-scan MS: resolution of 70,000 across 350 to 2000 mass/charge ratio, automatic gain control set to 3×10^6, and maximum injection time of 50 ms. The full MS scan was followed by MS/MS for the top 10 precursor ions in each cycle, with a normalized collision energy of 28 for unlabeled samples and 34 for TMT-labeled ones and a dynamic exclusion of 30 s. Raw mass spectral data files (.raw) were searched using Proteome Discoverer (Thermo Fisher Scientific) and MASCOT v2.4.1 (Matrix Science). MASCOT search parameters were as follows: 10–parts per million mass tolerance for precursor ions; 10 milli mass unit for fragment ion mass tolerance; two missed trypsin cleavages; fixed modifications: carbamidomethylation of cysteine and TMT 10plex modification of lysines and peptide N termini; variable modifications: oxidized methionine, Ser phosphorylation, Thr phosphorylation, and Tyr phosphorylation. Only peptides with a MASCOT score ≥25 and an isolation interference ≤30 were included in data analysis. TMT quantification was performed using Proteome Discoverer and isotopically corrected per manufacturer's instructions, and the values were normalized to the median of each channel. Phosphopeptides were manually validated using CAMV software (*58*).

Proteomics data analysis

After preprocessing and summing signals from multiple spectra of the same peptide, TMT reporter ion signals of all unique TRM9L peptides were selected, and, for each of the 10 channels, the geometric mean across all unique TRM9L peptides was calculated to represent the relative abundance of TRM9L across all 10 channels. This was repeated for each unique TRM9L phosphopeptide. The abundance of each phosphopeptide was normalized by dividing each channel value by the abundance of the TRM9L protein in that channel. This ratio was reported as the "relative degree of phosphorylation" for each phosphopeptide in each channel. Data represent means ± SD for three biological replicates. For comparing the degree of phosphorylation of a particular residue between two conditions, an unpaired Student's *t* test was performed ($P \leq 0.05$).

TRM9L binding partners

The coding region for TRM9L was cloned from complementary DNA (cDNA) isolated from HEK 293T cells. The S214A, S255A, and S214A/S255A mutants of TRM9L were generated by Gibson cloning. TRM9L constructs were cloned into a pcDNA3.1-FLAG-SBP expression vector or a pcDNA3.1-TWIN-STREP expression vector (*14*) S291A, and S380A mutants were PCR-amplified from FLAG constructs (under the "Cell line construction" section), cloned into pcDNA3.1-TWIN-STREP, and verified by Sanger sequencing. For stable expression, FLAG-SBP-TRM9L was cloned into pENTR.CMV.ON (Addgene, #32687) and then recombined into pLKO.DEST.hygro (Addgene, #32685) using Gateway LR clonase II Enzyme Mix (Life Technologies, 11791-020). The resulting pDest.hygro-FLAG-SBP-TRM9L plasmid was cotransfected with packaging plasmids (psPAX2 and pMD2.G) into 293T cells for lentivirus production. The 293T or SW620 cell lines were subsequently infected with the lentivirus in the presence of polybrene followed by stable clone selection using hygromycin.

Transient transfection and cellular extract production were performed as previously described (*14*). Whole-cell extract from transiently transfected cells cell lines (1 mg of total protein) was rotated with 20 µl of Anti-DYKDDDDK Magnetic Beads (Takara Bio USA, Clontech) or Strep-Tactin XT–coated magnetic beads (#2-4090-002, IBA GmbH) for 2 hours at 4°C in lysis buffer [20 mM Hepes-HCl (pH 7.9), 2 mM $MgCl_2$, 0.2 mM EGTA, 10% glycerol, 1 mM DTT, 0.1 mM phenylmethylsulfonyl fluoride, 0.1% NP-40, and 150 mM NaCl]. Resin was washed three times using the same buffer. Elution was carried out by acid elution [0.1 M glycine HCl (pH 2.68) and neutralized by tris-HCl (pH 8.5)] or boiling of beads in sample buffer for FLAG constructs. Elution for TWIN-STREP constructs was performed by using 5× biotin elution buffer (#2-1040-050, IBA GmbH) at a final concentration of 1× in lysis buffer. Cellular extracts and purified protein samples were fractionated on NuPAGE Bis-Tris polyacrylamide gels (Thermo Fisher Scientific), followed by transfer to an Immobilon-FL PVDF membrane (EMD Millipore) for immunoblotting using antibodies noted earlier. Immunoblots were scanned using direct infrared fluorescence on the Odyssey system (LI-COR Biosciences).

For silver staining compatible with MS, gels were fixed for 1 hour at ambient temperature in 40% ethanol/10% acetic acid. Gels were sensitized using 30% ethanol/0.2% sodium thiosulphate/6.8% sodium acetate. Three 5-min washes with H_2O followed. Gels were stained for 20 min with 0.25% silver nitrate followed by two 1-min washes with H_2O. The gel was developed with 2.5% sodium carbonate and 0.015% formaldehyde and stopped with 5% acetic acid. In-gel trypsin digestion and MS were carried out at the University of Rochester Medical Center Mass Spectrometry Resource Laboratory. After the digestion, sample was desalted with a C18 column and injected onto a Q Exactive Plus mass spectrometer operating in a data-dependent mode. Raw data were searched against the SwissProt human database (www.uniprot.org) using MaxQuant (Max Planck Institute of Biochemistry) to identify proteins.

Tumor formation assay

Fertilized White Leghorn chicken eggs (Charles River Laboratories) were incubated for 10 days at 37°C in a humidified atmosphere inside a hatching incubator equipped with an automatic rotator (Octagon 20, Brinsea). On the day of the experiment, each eggshell was punctured in two locations: the long side of the egg and the side over the natural air sac. Using a suction device, an artificial air sac was created to separate the CAM from the eggshell. A square window of ~1 cm was opened over the displaced CAM and sealed with a piece of sterile tape. SW620 cells expressing LacZ, WT TRM9L, and TRM9L mutants were detached from the plate with 2 mM EDTA in PBS and washed twice in PBS. Cells (5×10^5) were resuspended in 50 µl of PBS containing 1 mM $MgCl_2$, 0.5 mM $CaCl_2$, penicillin (100 U/ml), and streptomycin (100 µg/ml) and then inoculated into each CAM. The opening was resealed with tape, and the eggs were placed in a stationary incubator at 37°C for 7 days. The resulting tumors were excised and minced in a clean petri dish and then collagenased (type IA, Sigma-Aldrich) for 30 min at 37°C. The number of tumor cells was counted with a hemocytometer. Each data point represents an independent biological sample, with error bars representing SDs and statistical significance determined using a Mann-Whitney test.

SUPPLEMENTARY MATERIALS

Supplementary material for this article is available at http://advances.sciencemag.org/cgi/content/full/4/7/eaas9184/DC1

Supplementary Text

Fig. S1. TRM9L transcript level predicts clinical prognosis.

Fig. S2. TRM9L has a unique domain predicted to be intrinsically disordered and highly phosphorylated.

Fig. S3. MS/MS spectra of phosphorylated tryptic peptides from TRM9L.

Fig. S4. MS/MS spectra of phosphorylated tryptic peptides from TRM9L S380A mutant treated with H_2O_2.

Fig. S5. Copurification of 14-3-3 proteins with TRM9L is dependent on serine residues S214 and S255.

Fig. S6. Sensitivity of TRM9L expressing SW620 cells to the 14-3-3 antagonist BV02.

Fig. S7. Validation of TRM9L expression levels in SW620 stable cell lines.

Table S1. Kinase inhibitors screened for activity to block phosphorylation-dependent gel mobility shift of TRM9L.

REFERENCES AND NOTES

1. L.-X. Qin, Z.-Y. Tang, J. S. T. Sham, Z.-C. Ma, S.-L. Ye, X.-D. Zhou, Z.-Q. Wu, J. M. Trent, X.-Y. Guan, The association of chromosome 8p deletion and tumor metastasis in human hepatocellular carcinoma. *Cancer Res.* **59**, 5662–5665 (1999).
2. C. E. Gustafson, P. J. Wilson, R. Lukeis, E. Baker, E. Woollatt, L. Annab, L. Hawke, J. C. Barrett, G. Chenevix-Trench, Functional evidence for a colorectal cancer tumor suppressor gene at chromosome 8p22-23 by monochromosome transfer. *Cancer Res.* **56**, 5238–5245 (1996).
3. D. Birnbaum, J. Adélaïde, C. Popovici, E. Charafe-Jauffret, M.-J. Mozziconacci, M. Chaffanet, Chromosome arm 8p and cancer: A fragile hypothesis. *Lancet Oncol.* **4**, 639–642 (2003).
4. J. C. M. Pole, C. Courtay-Cahen, M. J. Garcia, K. A. Blood, S. L. Cooke, A. E. Alsop, D. M. L. Tse, C. Caldas, P. A. W. Edwards, High-resolution analysis of chromosome rearrangements on 8p in breast, colon and pancreatic cancer reveals a complex pattern of loss, gain and translocation. *Oncogene* **25**, 5693–5706 (2006).

5. J. M. Flanagan, S. Healey, J. Young, V. Whitehall, D. A. Trott, R. F. Newbold, G. Chenevix-Trench, Mapping of a candidate colorectal cancer tumor-suppressor gene to a 900-kilobase region on the short arm of chromosome 8. *Genes Chromosomes Cancer* **40**, 247–260 (2004).
6. L. M. Voeghtly, K. Mamula, J. L. Campbell, C. D. Shriver, R. E. Ellsworth, Molecular alterations associated with breast cancer mortality. *PLOS ONE* **7**, e46814 (2012).
7. J. Ashworth, B. Bernard, S. Reynolds, C. L. Plaisier, I. Shmulevich, N. S. Baliga, Structure-based predictions broadly link transcription factor mutations to gene expression changes in cancers. *Nucleic Acids Res.* **42**, 12973–12983 (2014).
8. U. Begley, M. S. Sosa, A. Avivar-Valderas, A. Patil, L. Endres, Y. Estrada, C. T. Y. Chan, D. Su, P. C. Dedon, J. A. Aguirre-Ghiso, T. Begley, A human tRNA methyltransferase 9-like protein prevents tumour growth by regulating LIN9 and HIF1-α. *EMBO Mol. Med.* **5**, 366–383 (2013).
9. B. Győrffy, A. Lanczky, A. C. Eklund, C. Denkert, J. Budczies, Q. Li, Z. Szallasi, An online survival analysis tool to rapidly assess the effect of 22,277 genes on breast cancer prognosis using microarray data of 1,809 patients. *Breast Cancer Res. Treat.* **123**, 725–731 (2010).
10. B. Győrffy, A. Lánczky, Z. Szállási, Implementing an online tool for genome-wide validation of survival-associated biomarkers in ovarian-cancer using microarray data from 1287 patients. *Endocr. Relat. Cancer* **19**, 197–208 (2012).
11. S.-L. Wang, J.-A. Huang, X.-Q. Liu, Mechanism of action of KIAA1456 gene on the proliferation and apoptosis of alveolar epithelial cells. *Eur. Rev. Med. Pharmacol. Sci.* **21**, 600–605 (2017).
12. H. M. Chen, J. Wang, Y. F. Zhang, Y. H. Gao, Ovarian cancer proliferation and apoptosis are regulated by human transfer RNA methyltransferase 9-likevia LIN9. *Oncol. Lett.* **14**, 4461–4466 (2017).
13. H. R. Kalhor, S. Clarke, Novel methyltransferase for modified uridine residues at the wobble position of tRNA. *Mol. Cell. Biol.* **23**, 9283–9292 (2003).
14. D. Fu, J. A. N. Brophy, C. T. Y. Chan, K. A. Atmore, U. Begley, R. S. Paules, P. C. Dedon, T. J. Begley, L. D. Samson, Human AlkB homolog ABH8 is a tRNA methyltransferase required for wobble uridine modification and DNA damage survival. *Mol. Cell. Biol.* **30**, 2449–2459 (2010).
15. L. Songe-Møller, E. van den Born, V. Leihne, C. B. Vågbø, T. Kristoffersen, H. E. Krokan, F. Kirpekar, P. Ø. Falnes, A. Klungland, Mammalian ALKBH8 possesses tRNA methyltransferase activity required for the biogenesis of multiple wobble uridine modifications implicated in translational decoding. *Mol. Cell. Biol.* **30**, 1814–1827 (2010).
16. J. Prilusky, C. E. Felder, T. Zeev-Ben-Mordehai, E. H. Rydberg, O. Man, J. S. Beckmann, I. Silman, J. L. Sussman, FoldIndex©: A simple tool to predict whether a given protein sequence is intrinsically unfolded. *Bioinformatics* **21**, 3435–3438 (2005).
17. F. Gnad, J. Gunawardena, M. Mann, PHOSIDA 2011: The posttranslational modification database. *Nucleic Acids Res.* **39**, D253–D260 (2011).
18. A. Bah, R. M. Vernon, Z. Siddiqui, M. Krzeminski, R. Muhandiram, C. Zhao, N. Sonenberg, L. E. Kay, J. D. Forman-Kay, Folding of an intrinsically disordered protein by phosphorylation as a regulatory switch. *Nature* **519**, 106–109 (2015).
19. L. M. Iakoucheva, P. Radivojac, C. J. Brown, T. R. O'Connor, J. G. Sikes, Z. Obradovic, A. K. Dunker, The importance of intrinsic disorder for protein phosphorylation. *Nucleic Acids Res.* **32**, 1037–1049 (2004).
20. O. Zugasti, W. Rul, P. Roux, C. Peyssonnaux, A. Eychene, T. F. Franke, P. Fort, U. Hibner, Raf-MEK-Erk cascade in anoikis is controlled by Rac1 and Cdc42 via Akt. *Mol. Cell. Biol.* **21**, 6706–6717 (2001).
21. P. Lassus, P. Roux, O. Zugasti, A. Philips, P. Fort, U. Hibner, Extinction of Rac1 and Cdc42Hs signalling defines a novel p53-dependent apoptotic pathway. *Oncogene* **19**, 2377–2385 (2000).
22. B. Zhao, L. Li, L. Wang, C.-Y. Wang, J. Yu, K.-L. Guan, Cell detachment activates the Hippo pathway via cytoskeleton reorganization to induce anoikis. *Genes Dev.* **26**, 54–68 (2012).
23. M. A. Loza-Coll, S. Perera, W. Shi, J. Filmus, A transient increase in the activity of Src-family kinases induced by cell detachment delays anoikis of intestinal epithelial cells. *Oncogene* **24**, 1727–1737 (2005).
24. S. T. Eblen, J. K. Slack, M. J. Weber, A. D. Catling, Rac-PAK signaling stimulates extracellular signal-regulated kinase (ERK) activation by regulating formation of MEK1-ERK complexes. *Mol. Cell. Biol.* **22**, 6023–6033 (2002).
25. K. Page, Y. Lange, Cell adhesion to fibronectin regulates membrane lipid biosynthesis through 5′-AMP-activated protein kinase. *J. Biol. Chem.* **272**, 19339–19342 (1997).
26. N. Dephoure, K. L. Gould, S. P. Gygi, D. R. Kellogg, Mapping and analysis of phosphorylation sites: A quick guide for cell biologists. *Mol. Biol. Cell* **24**, 535–542 (2013).
27. R. D. Guzy, B. Hoyos, E. Robin, H. Chen, L. Liu, K. D. Mansfield, M. C. Simon, U. Hammerling, P. T. Schumacker, Mitochondrial complex III is required for hypoxia-induced ROS production and cellular oxygen sensing. *Cell Metab.* **1**, 401–408 (2005).
28. E. O. Hileman, J. Liu, M. Albitar, M. J. Keating, P. Huang, Intrinsic oxidative stress in cancer cells: A biochemical basis for therapeutic selectivity. *Cancer Chemother. Pharmacol.* **53**, 209–219 (2004).
29. M. B. Sporn, K. T. Liby, NRF2 and cancer: The good, the bad and the importance of context. *Nat. Rev. Cancer* **12**, 564–571 (2012).
30. E. Piskounova, M. Agathocleous, M. M. Murphy, Z. Hu, S. E. Huddlestun, Z. Zhao, A. M. Leitch, T. M. Johnson, R. J. DeBerardinis, S. J. Morrison, Oxidative stress inhibits distant metastasis by human melanoma cells. *Nature* **527**, 186–191 (2015).
31. B. Halliwell, J. M. C. Gutteridge, *Free Radicals in Biology and Medicine* (Oxford Univ. Press, ed. 4, 2007).
32. T. Finkel, Signal transduction by reactive oxygen species. *J. Cell Biol.* **194**, 7–15 (2011).
33. M. Schieber, N. S. Chandel, ROS function in redox signaling and oxidative stress. *Curr. Biol.* **24**, R453–R462 (2014).
34. K. Z. Guyton, Y. Liu, M. Gorospe, Q. Xu, N. J. Holbrook, Activation of mitogen-activated protein kinase by H_2O_2. Role in cell survival following oxidant injury. *J. Biol. Chem.* **271**, 4138–4142 (1996).
35. A. Meves, S. N. Stock, A. Beyerle, M. R. Pittelkow, D. Peus, H_2O_2 mediates oxidative stress-induced epidermal growth factor receptor phosphorylation. *Toxicol. Lett.* **122**, 205–214 (2001).
36. I. Nakashima, K. Takeda, Y. Kawamoto, Y. Okuno, M. Kato, H. Suzuki, Redox control of catalytic activities of membrane-associated protein tyrosine kinases. *Arch. Biochem. Biophys.* **434**, 3–10 (2005).
37. A. Siebel, M. Cubillos-Rojas, R. C. Santos, T. Schneider, C. D. Bonan, R. Bartrons, F. Ventura, J. Rodrigues de Oliveira, J. L. Rosa, Contribution of S6K1/MAPK signaling pathways in the response to oxidative stress: Activation of RSK and MSK by hydrogen peroxide. *PLOS ONE* **8**, e75523 (2013).
38. C. M. Rosseland, L. Wierød, M. P. Oksvold, H. Werner, A. C. Østvold, G. H. Thoresen, R. E. Paulsen, H. S. Huitfeldt, E. Skarpen, Cytoplasmic retention of peroxide-activated ERK provides survival in primary cultures of rat hepatocytes. *Hepatology* **42**, 200–207 (2005).
39. R. Lara, M. J. Seckl, O. E. Pardo, The p90 RSK family members: Common functions and isoform specificity. *Cancer Res.* **73**, 5301–5308 (2013).
40. V. Oza, S. Ashwell, L. Almeida, P. Brassil, J. Breed, C. Deng, T. Gero, M. Grondine, C. Horn, S. Ioannidis, D. Liu, P. Lyne, N. Newcombe, M. Pass, J. Read, S. Ready, S. Rowsell, M. Su, D. Toader, M. Vasbinder, D. Yu, Y. Yu, Y. Xue, S. Zabludoff, J. Janetka, Discovery of checkpoint kinase inhibitor (*S*)-5-(3-fluorophenyl)-*N*-(piperidin-3-yl)-3-ureidothiophene-2-carboxamide (AZD7762) by structure-based design and optimization of thiophenecarboxamide ureas. *J. Med. Chem.* **55**, 5130–5142 (2012).
41. M. Saha, A. Carriere, M. Cheerathodi, X. Zhang, G. Lavoie, J. Rush, P. P. Roux, B. A. Ballif, RSK phosphorylates SOS1 creating 14-3-3-docking sites and negatively regulating MAPK activation. *Biochem. J.* **447**, 159–166 (2012).
42. J. A. Galan, K. M. Geraghty, G. Lavoie, E. Kanshin, J. Tcherkezian, V. Calabrese, G. R. Jeschke, B. E. Turk, B. A. Ballif, J. Blenis, P. Thibault, P. P. Roux, Phosphoproteomic analysis identifies the tumor suppressor PDCD4 as a RSK substrate negatively regulated by 14-3-3. *Proc. Natl. Acad. Sci. U.S.A.* **111**, E2918–E2927 (2014).
43. S. Chen, S. Synowsky, M. Tinti, C. MacKintosh, The capture of phosphoproteins by 14-3-3 proteins mediates actions of insulin. *Trends Endocrinol. Metab.* **22**, 429–436 (2011).
44. E. Wilker, M. B. Yaffe, 14-3-3 Proteins—A focus on cancer and human disease. *J. Mol. Cell. Cardiol.* **37**, 633–642 (2004).
45. A. K. Gardino, M. B. Yaffe, 14-3-3 proteins as signaling integration points for cell cycle control and apoptosis. *Semin. Cell Dev. Biol.* **22**, 688–695 (2011).
46. R. Anjum, J. Blenis, The RSK family of kinases: Emerging roles in cellular signalling. *Nat. Rev. Mol. Cell Biol.* **9**, 747–758 (2008).
47. P. Nowak-Sliwinska, T. Segura, M. L. Iruela-Arispe, The chicken chorioallantoic membrane model in biology, medicine and bioengineering. *Angiogenesis* **17**, 779–804 (2014).
48. E. I. Deryugina, J. P. Quigley, Chick embryo chorioallantoic membrane model systems to study and visualize human tumor cell metastasis. *Histochem. Cell Biol.* **130**, 1119–1130 (2008).
49. P. J. Roberts, C. J. Der, Targeting the Raf-MEK-ERK mitogen-activated protein kinase cascade for the treatment of cancer. *Oncogene* **26**, 3291–3310 (2007).
50. P. C. Dedon, S. R. Tannenbaum, Reactive nitrogen species in the chemical biology of inflammation. *Arch. Biochem. Biophys.* **423**, 12–22 (2004).
51. W. C. Lee, C. H. Choi, S. H. Cha, H. L. Oh, Y. K. Kim, Role of ERK in hydrogen peroxide-induced cell death of human glioma cells. *Neurochem. Res.* **30**, 263–270 (2005).
52. P. O'Neill, Radiation-induced damage in DNA, in *Radiation Chemistry: Present Status and Future Trends*, C. D. Jonah, B. S. M. Rao, Eds. (Elsevier Science, 2001), vol. 87, pp. 585–622.
53. E. I. Azzam, J.-P. Jay-Gerin, D. Pain, Ionizing radiation-induced metabolic oxidative stress and prolonged cell injury. *Cancer Lett.* **327**, 48–60 (2012).
54. S. Desaint, S. Luriau, J.-C. Aude, G. Rousselet, M. B. Toledano, Mammalian antioxidant defenses are not inducible by H_2O_2. *J. Biol. Chem.* **279**, 31157–31163 (2004).
55. V. G. Tusher, R. Tibshirani, G. Chu, Significance analysis of microarrays applied to the ionizing radiation response. *Proc. Natl. Acad. Sci. U.S.A.* **98**, 5116–5121 (2001).
56. S. Stöcker, K. Van Laer, A. Mijuskovic, T. P. Dick, The conundrum of hydrogen peroxide signaling and the emerging role of peroxiredoxins as redox relay hubs. *Antioxid. Redox Signal.* **28**, 558–573 (2018).

57. S. B. Ficarro, G. Adelmant, M. N. Tomar, Y. Zhang, V. J. Cheng, J. A. Marto, Magnetic bead processor for rapid evaluation and optimization of parameters for phosphopeptide enrichment. *Anal. Chem.* **81**, 4566–4575 (2009).
58. T. G. Curran, B. D. Bryson, M. Reigelhaupt, H. Johnson, F. M. White, Computer aided manual validation of mass spectrometry-based proteomic data. *Methods* **61**, 219–226 (2013).

Acknowledgments: We thank A. Del Rosario and R. Schiavoni for assistance with phosphoproteomics at the Proteomics Core of Massachusetts Institute of Technology Koch Institute Swanson Biotechnology Center and Y. Li for assistance with the cloning of TRM9L mutants. **Funding:** C.G. was supported by a David H. Koch Cancer Fellowship, a Howard Hughes Medical Institute International Student Research Fellowship, and a Siebel Scholarship. D.F. was supported by NSF CAREER Award 1552126. T.J.B. and P.C.D. were supported by grants ES026856 and ES024615 from the National Institute of Environmental Health Sciences. P.C.D. was also supported by grant CA026731 from the National Cancer Institute. **Author contributions:** C.G. participated in study design, performing the bulk of the experiments, interpreting data, and manuscript writing. J.R. designed and executed the 14-3-3 studies, interpreting data and manuscript writing. U.B. constructed TRM9L cell lines, performed xenograft studies, and contributed to study design and manuscript writing. D.F., T.J.B., and P.C.D. contributed to study design, data interpretation, and manuscript writing. **Competing interests:** The authors declare that they have no conflicts of interest with the contents of this article. The content is solely the responsibility of the authors and does not necessarily represent the official views of NIH. **Data and materials availability:** MS data were deposited in Chorus (www.chorusproject.org) project ID 1336: Experiment *Phosphorylation sites of TRM9L in HCT116 cells*, Experiment *Phosphorylation of TRM9L WT and S380A mutant under H2O2 treatment*, Experiment *Dynamics of TRM9L phosphorylation under H2O2 treatment*, and Experiment *Binding partners of ALKBH8 and TRM9L in HEK293 cells*. All data needed to evaluate the conclusions in the paper are present in the paper and/or the Supplementary Materials. Additional data related to this paper may be requested from the authors.

Submitted 4 January 2018
Accepted 1 June 2018
Published 11 July 2018
10.1126/sciadv.aas9184

Citation: C. Gu, J. Ramos, U. Begley, P. C. Dedon, D. Fu, T. J. Begley, Phosphorylation of human TRM9L integrates multiple stress-signaling pathways for tumor growth suppression. *Sci. Adv.* **4**, eaas9184 (2018).